Improving the Barrier Properties of Thermoplastic Corn Starch-based Films Containing Bacterial Cellulose Nanowhiskers by Means of PHA Electrospun Coatings of Interest in Food Packaging

María José Fabra[*], *Amparo López-Rubio, Jesús Ambrosio-Martín, and Jose M. Lagaron*

Novel Materials and Nanotechnology Group, IATA-CSIC, Avda. Agustin Escardino 7, 46980 Paterna (Valencia), Spain, email: mjfabra@iata.csic.es

Highlights

- BCNW were incorporated into thermoplastic corn starch nanocomposites (TPCS)
- Colourless TPCS/BCNW nanocomposites were prepared by melt blending process
- BCNW enhanced oxygen barrier up to 95% as compared to the neat TPCS
- Multilayer structures based on TPCS/BCNW films and PHA/BCNW coatings were developed
- Barrier properties of the multilayer structures thus obtained were significantly improved

Abstract

In the present study, property enhanced thermoplastic corn starch (TPCS) nanobiocomposites containing bacterial cellulose nanowhiskers (BCNW) prepared by melt mixing were characterized in terms of morphology, mechanical, optical and barrier properties. Improved barrier to water vapour and oxygen at high relative humidity (80%) was noticed, reaching the best performance at 15 wt% BCNW loading with a maximum drop of 46% and 95% for water and oxygen permeability, respectively. In a second approach, the optimized nanobiocomposites (containing 15 wt% BCNW) were successfully hydrophobized by coating them with electrospun poly(3-hydroxybutyrate) (PHB) or electrospun PHB-BCNW fibres. To this end, hybrid electrospun PHB fibres reinforced with highly dispersed crystalline BCNW in solutions concentrations up to 15 wt% were directly electrospun onto both sides of TPCS nanobiocomposites containing 15 wt% BCNW. Similar coated structures prepared without BCNW were developed and characterized for comparative purposes. The methodology used resulted in good adhesion between the layers, also leading to enhanced barrier performance. Interestingly, the incorporation of BCNW in one of the layers led to a decrease on the oxygen permeability values showing no significant differences between multilayer films incorporating BCNW whatever the layer where the BCNW were located. However, when comparing amongst the different multilayer samples containing BCNW, the greatest reduction in the water vapour permeability values was seen for multilayer structures incorporating BCNW in both, the TPCS inner layer and the PHB coating. This study has demonstrated the potential of the combination of both technologies (nanocomposites and multilayered design) in the development of food packaging materials based on corn starch with improved barrier properties

Keywords: BCNW, Nanobiocomposites, Multilayers, Corn Starch, Barrier Properties, Electrospinning.

1. INTRODUCTION

The increasing demand for biodegradable plastics for packaging based on renewable resources has led to the consideration of polysaccharide and proteins as raw materials. One of the major constraints when replacing synthetic polymers with natural ones is that, in most cases, films cannot be produced using industrial processes by means of extrusion, melt-mixing or other processing equipments because they are not thermoplastic materials and they can be degraded during thermal processing. Some of these biopolymers are manufactured by casting, which involves drying times that are too long to permit large-scale manufacturing (Fabra *et al*., 2011, Jiménez *et al.,* 2012a, Liew and Ramesh, 2015). As a solution to this problem, the production of starch composites by thermoplastic treatment is an interesting option. Starch, a natural polymer, is one of the most promising candidates especially due to its attractive combination of low price, wide availability, high purity, non-toxicity and biodegradability and environmental compatibility (Xu, Kimb, Hanna and Nag, 2005). Although native starch is not a thermoplastic material, it can be processed like conventional polymers after some pre-processing. Starch granules do not possess thermoplastic character in its pristine form unless they are completely or partially destroyed and transformed into an amylose/amylopectin semicrystalline matrix under high temperature and/or pressure and in the presence of plasticizers (Van Soest, Hulleman, de Wit, and Vliegenthart, 1996, Jiménez *et al*., 2012b, Mendes *et al*., 2016). Plasticizers not only play an important role in processing, but also in improving the mechanical properties of starch-based films. From the evidence that the properties of thermoplastic starch (TPS) are highly dependent on the moisture and plasticizer contents, it has to be considered that in the particular case of food packaging applications, where gas permeability is a key factor for the packaged product shelf-life,

100 it is necessary to select the correct type and amount of plasticizer in order to obtain a
101 good balance between mechanical and barrier performance for each particular
102 application. Different approaches have been widely studied in order to improve TPS
103 mechanical and barrier performance and to reduce its hydrophilic character which
104 strongly handicap their use in food packaging applications. In fact, the tendency in the
105 market is the production of starch-based materials with a high content of starch together
106 with other biodegradable plastics (30-80%), either by using blends (Alvarez *et al.*, 2004,
107 Avérous *et al.*, 2000, Carmona *et al.*, 2014, Lai *et al.*, 2005) or through the addition of
108 dispersed nanoreinforcing agents to generate nanobiocomposites (Park *et al.*, 2002,
109 Dean *et al.*, 2008, Mohan and Kanny, 2016, Zeppa *et al.*, 2009).
110 Hence, from an application point of view, it is of great relevance to tailor the properties
111 of thermoplastic starch, with special focus on their barrier performance, and to enhance
112 the overall functionalities to make them more adequate for food packaging applications
113 without compromising their inherently good properties (i.e. transparency) and
114 biodegradability. To overcome these issues, two main approaches have been proposed
115 in this work. The first one consists on the development of nanobiocomposite materials
116 through the addition of bacterial cellulose nanowhiskers (BCNW) into the thermoplastic
117 corn starch (TPCS) films by direct melt compounding. In this case, BCNW must
118 provide a good matrix-filler adhesion and high nanofiller dispersion within the
119 biopolymeric matrix. The second one consists on adjusting the properties of the
120 thermoplastic starch and nanobiocomposites by developing multilayer structures based
121 on the electrospinning process as it has been previously reported by Fabra *et al.*,
122 2015ab. It is worth mentioning that multilayer structures have been widely used in
123 synthetic polymers but they have been barely developed in biodegradable food
124 packaging systems since it is difficult to assemble materials thermodynamically

immiscible without the addition of synthetic adhesives. In this regard, the main challenge is to develop biodegradable coatings which favor the adhesion between layers and this can be achieved by the application of the electrospinning process with the additional advantage that it is an easily scalable technique which could facilitate the real application of the biodegradable polymers in the food packaging industry. To this end, the nanobiocomposites were hydrophobized by coating them with electrospun poly(3-hydroxybutyrate) (PHB) fibers containing or not BCNW in order to keep the oxygen barrier properties that the TPCS possesses at low relative humidity but, in this case, at high humidity, i.e. in real packaging conditions.

Therefore, the novelty of this work relies on establishing a new bio-based multilayer concept based on a starch-based nanocomposite film coated with cellulose nanowhiskers-containing PHA electrospun fibers. The development of multilayer structures including nanocellulose-containing fibers has not been reported before and it shows an advantage versus incorporation of neat fibers.

2. MATERIALS AND METHODS

2.1 Materials

High-amylose corn starch (amylose content ≥ 80%) was kindly supplied by Roquette (Roquette Laisa España, Benifaio, Spain) and glycerol was purchased from Panreac Quimica, S.A. Castellar Del Vallés, Barcelona, Spain. Poly(3-hydroxybutyrate) (PHB) was supplied by Biomer (Krailling, Germany). 2,2,2-Trifuoroethanol (TFE) with 99 % purity was purchased from Sigma-Aldrich (Spain). All products were used as received without further purification.

Sulphuric acid 96 wt% and sodium hydroxide pellets were purchased from Panreac (Barcelona, Spain). The bacteria strain *G. xylinus* was obtained from the Spanish type culture collection (CECT).

2.2. Preparation of films

2.2.1 Preparation bacterial cellulose nanowhiskers (BCNW).

Initially, bacterial cellulose mats were obtained using the bacterial strain *Gluconacetobacter xylinus 7351* as described in previous works (Ambrosio-Martin *et al*., 2015, Martínez-Sanz *et al*., 2011). After that BCNW were obtained by acid hydrolysis using the optimized method reported by Martinez-Sanz *et al*., 2011. Full description of the synthesis of the BCNW can be found elsewhere (Martinez-Sanz *et al*., 2011). Briefly, small pieces of bacterial cellulose at neutral pH were ground in a blender. A gel-like material was then obtained and compressed in order to remove most of the absorbed water. The partially dried cellulosic material was then treated with 301 mL sulfuric acid/L water, in a cellulose/acid ratio of approximately 7 $g \cdot L^{-1}$, at 50 ºC for 2 days, until homogenous solution was obtained. The cellulose nanowhiskers were obtained as a white precipitate after several centrifugations and washing cycles at 12.500 rpm and 15 ºC for 20 min. The pH of the samples was measured after the washing-centrifugation cycles, being around two for all the samples. Then, the material was re-suspended in deionized water and neutralized with sodium hydroxide until neutral pH and, subsequently, centrifuged to obtain the final product as a partially hydrated precipitate which was kept refrigerated. This last step was thought to turn the filler heat stable.

2.2.2 Preparation thermoplastic corn starch based films (TPCS) and TPCS-BCNW

nanobiocomposites.

Corn starch and glycerol, as plasticizer, were dispersed in water using a polymer: glycerol: water weight ratio of 1:0.3:0.5 and the dispersion was melt-mixed in a Brabender Plastograph internal mixer at 130ºC and 60 rpm for 4 minutes. The starch:glycerol:water ratio was determined according to the minimum amount of plasticizer need to turn the material thermoplastic. To this end, based on screening studies the amount of glycerol and water was optimized since barrier properties (i.e. water vapour and oxygen) of starch based films can be detrimentally affected by increasing the plasticizer amount. The mixture was then spread evenly on Teflon and placed in a compression mould (Carver 4122, USA) at a pressure of 2MPa and 130ºC for 5 minutes.

Nanobiocomposites TPCS/BCNW films were identically prepared but, in this case, the corn starch:glycerol:water dispersions were melt-mixed with 2, 5, 10, 15 or 20 wt% BCNW with respect to the TPCS weight, and they were subsequently compression moulded into films using the hot-plate hydraulic press (130 ºC and 2MPa for 5 min).

2.2.2 Preparation of nanostructured PHB/BCNW coatings.

Electrospun hybrid fibres were generated from PHB-BCNW solutions in TFE. Based on a previous work (Martínez-Sanz *et al*., 2014), these solutions contained a total solids content of 4 wt% and the BCNW concentration was 15 wt% BCNW, regarding the PHB weight.

Firstly, in order to guarantee a better dispersion of the BCNW into the PHB matrix, a solvent-exchanged procedure with acetone and TFE was used for the partially hydrated BCNW. The solvent-exchanged BCNW was subsequently dispersed by applying intense homogenization (Ultra-Turrax) for 2 minutes and sonification for 30 s and then,

198 stirred with the PHB at 40 ºC. For comparative purposes, an identically prepared PHB
199 solution but without the BCNW was also used as a coating.
200 The electrospinning apparatus was a Fluidnatek^{TM} basic equipment, manufactured by
201 Bioinicia S.L. (Paterna, Spain) equipped with a variable high voltage 0-30 kV power
202 supply and a horizontal flat collector were the TPCS and nanobiocomposites films were
203 located. Solutions were transferred to 5 mL plastic syringes and connected through a
204 PTFE tube to a stainless steel needle (ϕ 0.9 mm). The syringe was lying on a digitally
205 controlled syringe pump while the needle was in horizontal towards a stainless steel
206 plate collectorand the solvent was vented out of the chamber during the electrospinning
207 run. The experiment was carried out at ambient conditions (23°C and 40% RH). The
208 distance between the needle and the collector was 10 cm and the voltage was 14 kV.
209 The flow rate was 0.6 mL/h.
210
211 **2.2.3 Preparation of multilayer structures.**
212 PHB or PHB/BCNW fibre mats were directly electrospun onto both sides of the TPCS
213 or nanobiocomposite films containing 15 wt% BCNW. Thus, four different multilayer
214 systems were prepared (see Table 1) and the total amount of electrospun material (~
215 0.62 ± 0.09 mg cm^{-1}) was estimated by weighing the nanobiocomposite film before and
216 after deposition of the electrospun material.
217 With the double aim of promoting fibers coalescence into a homogeneous film and of
218 improving the adhesion between layers, an additional annealingstep was applied. To this
219 end TPCS and nanobiocomposite films were placed between hot plates at 160ºC for 1
220 min.
221
222 **2.2.4. Film equilibration and storage**

223 Prior to testing, nanocomposite films and multilayer structures were equilibrated in
224 desiccators at 25 ºC and 0% RH, by using dried silica gel for one week.
225
226 **2.3. Characterization of films**
227 **2.3.1. Scanning Electron Microscopy (SEM)**
228 SEM was conducted on a Hitachi microscope (Hitachi S-4800) at an accelerating
229 voltage of 5 kV and a working distance of 14 mm. TPCS films as well as the
230 electrospun coated multilayer systems were cryo-fractured after immersion in liquid
231 nitrogen and subsequently sputtered with a gold–palladium mixture under vacuum
232 before their morphology was examined using SEM.
233
234 **2.3.2. Optical microscopy**
235 Polarized light microscopy (PLM) examinations were performed using a Nikon Eclipse
236 90i optical microscope (IZASA, Spain) equipped with 5-megapixels cooled digital
237 colour microphotography camera Nikon Digital Sight DS-5Mc. Captured images were
238 analysed and processed by using Nis-Elements Br software.
239
240 **2.3.3. Tensile properties**
241 Tensile tests were performed according to ASTM Standard D638 (ASTM 2010) in
242 stamped dumbbell-shaped specimens of the samples. An Instron Testing Machine
243 (Model 4469; Instron Corp., Canton, MA, USA) was used, with a crosshead speed of 10
244 mm/min, at ambient conditions of typically 24°C and 50% RH. Elastic Modulus (E),
245 Tensile Strength (TS), and Elongation at Break (EAB) were determined from the stress-
246 strain curves, estimated from force–distance data obtained for the different films. At

least, four specimens of each film were tensile tested as to obtain statistically meaningful results.

2.3.4. Water vapour permeability (WVP)

Water vapour permeability (WVP) was measured, in triplicate, according to the ASTM (1995) gravimetric method, using Payne permeability cups (Elcometer SPRL, Hermelle/s Argenteau, Belgium). Distilled water was placed inside the cup to expose the film (the exposed area was 9.6×10^{-4} m^2) to 100% RH on one side. Once the films were secured, each cup was placed in an equilibrated relative humidity cabinet at 0% RH and 25°C. The cups were weighed periodically (±0.0001 g). Cups with aluminium films were used as control samples to estimate solvent loss through the sealing. Water vapour permeation rate was calculated from the steady-state permeation slopes obtained from the regression analysis of weight loss data vs. time, and weight loss was calculated as the total cell loss minus the loss through the sealing. Permeability was obtained by multiplying the permeance by the average film thickness.

2.3.5. Oxygen permeability (OP)

The oxygen permeability coefficient was derived from oxygen transmission rate (OTR) measurements recorded using an Oxygen Permeation Analyzer 8001 (Systech Illinois, UK). Experiments were carried out at 24°C and 80% RH. The samples were previously purged with nitrogen in the humidity equilibrated samples, before exposure to an oxygen flow of 10 mL min^{-1}. The exposure area during the test was 5 cm^2 for each sample. In order to obtain the oxygen permeability, film thickness and gas partial pressure were considered in each case. The measurements were done in duplicate.

2.3.6 Contact angle measurements

Measurements of contact angle were carried out at 23 ± 2ºC and ambient relative humidity (*ca.* 60%RH) in a Video-Based Contact Angle Meter model OCA 20 (DataPhysics Instruments GmbH, Filderstadt, Germany). Contact angle measurements were obtained by analyzing the shape of a distilled water drop after it had been placed over the film for 15 s. Image analyses were carried out by SCA20 software.

2.3.7 Optical Properties.

The transparency of the films was determined through the surface reflectance spectra in a spectrocolorimeter CM-3600d (Minolta Co., Tokyo, Japan) with a 10 mm illuminated sample area. Measurements were taken in triplicate for each sample by using both a white and a black background. Film transparency was evaluated through the internal transmittance (T_i) (0–1, theoretical range) by applying the Kubelka–Munk theory for multiple scattering to the reflection data. Internal transmittance (T_i) of the films was quantified using equation (1). In this equation, R_0 is the reflectance of the film on an ideal black background. Parameters a and b were calculated by equations. (2) and (3), where R is the reflectance of the sample layer backed by a known reflectance R_g.

$$T_i = \sqrt{(a - R_0)^2 - b^2} \quad (1)$$

$$a = \frac{1}{2} \cdot \left(R + \frac{R_0 - R + R_g}{R_0 R_g} \right) \quad (2)$$

$$b = \left(a^2 - 1\right)^{1/2} \quad (3)$$

2.4. Statistical Analysis.

One-way analysis of the variance (ANOVA) was performed using Statgraphics Plus for Windows 5.1 (Manugistics Corp., Rockville, MD). Fisher's least significant difference (LSD) was used at the 95% confidence level.

295

296 ## 3. RESULTS AND DISCUSSION

297 ### 3.1 Development of starch-BCNW nanobiocomposites

298 The main objective of the first part of this work was to produce nanobiocomposite
299 materials based on thermoplastic corn starch matrices and using BCNW as nanofillers
300 which were produced by sulphuric acid hydrolysis of bacterial cellulose pellicles. These
301 nanofillers showed a high aspect ratio (*ca.* 30), high crystallinity (*ca*. 95% crystallinity
302 index) and thermal stability (degradation temperature of ca. 317ºC) (Martínez-Sanz *et*
303 *al*., 2011).

304 Figure 1 shows the contact transparency images of the TPCS based films and of their
305 nanobiocomposites containing BCNW. As observed, all the materials presented a good
306 contact transparency, which was not compromised by the addition of BCNW. The
307 transparency was also quantitatively assessed by means of internal transmittance (Ti)
308 measurements. This parameter is directly related to the arrangement of film´s
309 components and thus, to the surface and the internal structure of the developed material.
310 Therefore, the transparency is greatly affected by the morphology and particle size
311 distribution which is, in turn, directly linked to the light transmission/dispersion
312 behavior of the nanobiocomposite films (Fabra *et al*., 2009). It is generally assumed that
313 an increase in Ti values is related to more homogeneous and transparent films while a
314 decrease in these values implies a greater light dispersion, greater opacity and thus more
315 heterogeneous matrices.

316 From Figure 2, a similar pattern was observed between TPCS based films and those
317 containing BCNW, and only small differences were detected in the internal
318 transmittance values. This decrease in transparency could be attributed to the presence
319 of BCNW resulting in different refractive index.

To examine the morphology of the neat TPCS and of the nanobiocomposites films as well as the BCNW dispersion, the cryo-fractured surface of the developed nanobiocomposites were observed by SEM and representative micrographs of each film are displayed in Figure 3. The pure TPCS film was continuous and homogeneous with a smooth surface while BCNW addition affected the film microstructure. BCNW could be easily identified since they appeared either as white dots or forming bundles. At low loadings, nanofillers were properly dispersed and distributed in the TPCS matrix but rougher cross-sections were observed at greater BCNW loadings. It seems that nanocomposites containing 5 wt% BCNW showed the better BCNW dispersion while higher concentrations induced some agglomerations of the BCNW and they were not properly dispersed within the biopolymer matrix. Observations of the different nanobiocomposites films by optical microscopy with polarized light (*cf.* Figure 4) confirmed that increasing the nanofiller content, led to a decrease in BCNW dispersion.

Table 2 gathers the tensile properties of TPCS and its nanobiocomposite films. From these results it can be concluded that the addition of BCNW resulted in a stiffening of the materials reflected by an increase in the elastic modulus. A similar behaviour was previously reported by Kvien *et al.*, 2007 for modified potato starch nanocomposites containing cellulose nanowhiskers (CNW). BCNW had a major effect on the elastic modulus for all nanobiocomposite films while the elongation at break slightly decreased in nanobiocomposites with low loadings of BCNW compared to the neat TPCS matrix and this reduction became significant (*ca.* 50% reduction) for higher BCNW loading (15 and 20 wt%), turning the material less stretchable. This could be ascribed to both the high filler-matrix interfacial adhesion due to the hydrophilic nature of the BCNW and TPCS and, on the other hand, to the filler-filler interactions (Martínez-Sanz *et al.*, 2013; Azizi Samir *et al.* 2005; George *et al.*, 2011). Other works also reported the

345 increased E and TS values for melt processed biopolymers such as PLA incorporating
346 high amounts of cellulosic fillers (Fortunati *et al*., 2010) together with a reduction in the
347 elongation at break. It is known that the addition of reinforcing agents in biopolymeric
348 materials results in a reduction of E values since nanofillers act as stress concentrating
349 components. Therefore, the addition of BCNW to TPCS based films resulted in an
350 improvement of the mechanical properties (E and TS) which can be linked not only to
351 the good nanofiller dispersion in the matrix, resulting from the chemical similarity, but
352 also the strong nanofiller-matrix adhesion by hydrogen bonding interactions. Similar
353 behaviour has been previously reported for starch based nanocomposites reinforced with
354 flax cellulose nanocrystals (Cao *et al*., 2008; Xie *et al*., 2013).
355 Table 2 summarizes the measured water vapour permeability (WVP) for the neat TPCS
356 and its nanobiocomposites. The WVP of the neat TPCS was lower than that previously
357 reported for the corn starch cast films (Jiménez *et al*., 2012b). All the TPCS
358 nanobiocomposites incorporating BCNW had significantly lower WVP, with a
359 maximum permeability drop of 46 % for the 15 %BCNW loading, as compared to the
360 neat TPCS. Similar effects were previously observed in gelatin reinforced with BCNW
361 (George and Siddaramaiah, 2012) and hydroxypropyl methylcellulose (HPMC)
362 reinforced with microcrystalline cellulose (Bilbao-Sáinz *et al*., 2011).
363 Oxygen permeability was measured at 80% RH and the results are also gathered in
364 Table 2. The oxygen permeability values for the neat TPCS are in agreement with those
365 reported in the literature (Jiménez *et al*., 2012b; Müller *et al*., 2011). The first clear
366 observation is that by increasing the BCNW content, TPCS-based nanobiocomposite
367 films presented significantly enhanced oxygen barrier properties. However, the
368 nanobiocomposites which presented the best oxygen barrier performance were those
369 with 15 wt% BCNW. These results highlight that, up to 15 wt% loading, the

improvement in the oxygen barrier properties could be ascribed to the BCNW content. Nevertheless, higher BCNW loadings did not decrease the oxygen permeability values of the nanobiocomposite films probably due to an excess of BCNW agglomerates. In fact, proportionally, the percentage of reduction was higher for 2 and 5 wt% BCNW related to the better dispersion achieved for these BCNW contents. Not surprisingly, increasing the amount of waterproof BCNW blocks incorporated led to improved oxygen barrier properties. However, the most important reduction was observed at low BCNW concentrations.

3.2 Development of multilayer TPCS-based films

Despite of improving barrier and tensile properties of the TPCS-based films by the addition of BCNW, one of the main drawbacks of these hydrophilic materials is that they present higher water and oxygen permeability values at high relative humidity conditions than other biodegradable polymers (polylactic acid –PLA- or polyhydroxyalkanoates –PHA-) or synthetic ones. Therefore, moisture resistant TPCS-based films are needed in order to broaden the application window of these films. To overcome this problem, the use of multilayer structures, in which TPCS films are coated with hydrophobic biopolymers based on PHB was proposed in this work as a feasible route. Based on the results obtained in the first part of this study, the nanobiocomposite film containing 15 wt% of BCNW were chosen as an inner layer of the multilayer structure according to the better oxygen and water vapour barrier properties obtained in this case. Three-layer films were prepared and compared by combining the use of BCNW as an additive of the inner layer and/or the PHB coating outer layers. PHB fibres containing or not BCNW were directly electrospun onto both sides of TPCS-based films or its nanobiocomposites prepared with 15 wt% BCNW. Figure 5 displays a

representative SEM image of a three-layer film formed by means of the electrospinning process in which a laminate-like structure was observed. It was clearly observed that the outer layers were thinner than the inner, showing excellent adhesion between them. In this particular case, the internal structure of each layer was quite heterogeneous due to the presence of BCNW nanofillers in each layer.

Figure 6 shows the contact transparency images of the obtained TPCS multilayer structures. As observed, all hybrid films showed a similar contact transparency, which was slightly different to the neat TPCS (see Figure 1). These results agreed with those found for internal transmittance values in which a significant reduction was noticed for multilayer films (see Table 3 Ti values, measured at 550 nm). Over the wavelengths considered, multilayer samples showed similar internal transmittance patterns than TPCS and its nanocomposites. Therefore, only the internal transmittance values measured at 550nm are given in this case. As deduced from Table 3, the internal transmittance reduction was enhanced by the presence of BCNW which was caused by the scattering of the nanofillers. In any case, internal transmittance spectra were above 75 % for all the samples indicating good transparency of the films.

The mechanical properties of multilayer structures are summarized in Table 3. In general, the multilayer films exhibited a higher Young´s Modulus than the TPCS and its nanobiocomposites containing 15 wt% BCNW, regardless of the composition of the coating (outer layers). It is also important to highlight the reinforcing effect that the BCNW had when they were included in the PHB coating, showing greater E values than their counterparts prepared without BNCW. An embrittlement of the TPCS and TPCS-15%BCNW was observed for all samples with a decrease in the tensile strength upon the addition of the outer layers (*cf.* Table 2 and Table 3) although no significant differences were observed between multilayer samples. Finally, the elongation at break

of multilayer structures, in general, was greater indicating that the outer PHB layers somehow plasticized the inner layer, thus leading to higher EAB values and lower TS. In contrast, the incorporation of the biopolyester coatings (both with or without the nanofiller), resulted in greater E values indicating that these outer layers had a reinforcing effect in the elastic zone of the materials.

As compared to commercial packaging materials, the developed multilayer structures are less deformable and more flexible and elastic than high or low-density polyethylene (HDPE and LDPE) or polypropylene. LDPE and HDPE samples present EAB values of ca. 300 and 500%, respectively while the tensile strength was found to range between 9-17 and 17-35, respectively (Bristol, 1986).

Table 3 gathers water vapour and oxygen permeability for the developed films. The first observation to highlight is that both water and oxygen barrier properties were significantly improved by the addition of PHB and PHB/BCNW although oxygen permeability was improved to a greater extent. Interestingly, the incorporation of BCNW either in the inner, outer or both layers, led to a decrease in the oxygen permeability values showing no significant differences between three-layer films incorporating BCNW whatever the layer where the BCNW were located. However, when comparing amongst the different multilayer samples containing BCNW, the greatest reduction in the water vapour permeability values was seen for three-layer films incorporating BCNW in both, the TPCS layer and the PHB coating.

Bearing in mind the water vapour and oxygen permeability values of the pure TPCS and its nanobiocomposite containing 15 wt% BCNW (see Table 2), the permeability drop, after coating these materials with PHB, was greater for the multilayer structures prepared with TPCS as inner layer, reaching permeability reductions of up to 70 and 98% for the water vapour and oxygen permeability, respectively. However, the

445 permeability reductions in their counterparts prepared with TPCS with 15% of BCNW
446 were 46 and 67% for water vapour and oxygen barrier properties, respectively.
447 Moreover, the wettability properties of the neat TPCS, TPCS-15%BCNW
448 nanobiocomposite and the coated multilayer systems were determined by direct
449 measurement of contact angles of a water drop deposited on the upper surface of
450 samples and the results are listed in Table 3. The contact angle of the neat TPCS and its
451 nanobiocomposite film was 54.8 ± 3.4º and 52.2 ± 2.0º, respectively. However, PHB
452 and PHB/BCNW outer layers were quite effective in protecting the water sensitive inner
453 layer from outside moisture.
454 Finally, if permeability data are compared with those reported for synthetic materials
455 commonly used in the food industry, the developed multilayer structures showed lower
456 barrier properties than those of polyethylene terephthalate (PET) but in the same range
457 of low-density polyethylene (OP $2.22*10^{-17}$ $m^3 \cdot m \cdot m^{-2} \cdot s^{-1} \cdot Pa^{-1}$) which is the main film
458 used for packaging fresh fruits and vegetables.
459

460 **4. CONCLUSIONS**

461 In this work, thermoplastic corn starch (TPCS) nanobiocomposites containing bacterial
462 cellulose nanowhiskers (BCNW) were successfully developed by direct melt-mixing
463 and they were characterized in terms of morphological, optical, barrier and tensile
464 properties. Morphological studies corroborated that the BCNW were properly dispersed
465 into the TPCS matrix up to 15 wt% loading with the subsequent improvement in barrier
466 properties. The addition of BCNW resulted in a stiffening of the materials reflected by
467 an increase in the elastic modulus. The elongation at break slightly decreased in
468 nanobiocomposites with low loadings of BCNW compared to the neat TPCS matrix and

this reduction became significant (*ca*. 50% reduction) for greater BCNW loadings (15 and 20 wt%), turning the material less stretchable.

In the second part of this work, an innovative strategy was used, involving the coating of the nanobiocomposites films by electrospun poly(3-hydroxybutyrate) (PHB) fibers homogenized by annealing, in order to protect the nanobiocomposite from moisture. Barrier properties of the multilayer structures thus obtained were significantly improved.

Acknowledgments

The authors acknowledge financial support from MINECO (AGL2015-63855-C2-1project). M.J. Fabra is recipient of a Ramon y Cajal contract (RYC-2014-158) from the Spanish Ministry of Economy and Competitiveness.

REFERENCES

Alvarez, V.A., Frage, A.N. and Vazquez, A. (2004). Effects on the moisture and fibre content on the mechanical properties of biodegradable polymer-sisal fiber biocomposites. *Journal of Applied Polymer Science*, 91, 4007-4016.

Ambrosio-Martín, J.; Fabra, M. J.; López-Rubio, A.; Lagarón, J. M. (2015). Melt polycondensation to improve the dispersion of bacterial cellulose into polylactide via melt compounding: enhanced barrier and mechanical properties. *Cellulose*, 22,1201–1226.

ASTM. (1995). Standard test methods for water vapour transmission of materials. Standars designations: E96–95. In Annual book of ASTM standards (pp. 406–413). Philadelphia: American Society for Testing and Materials.

493 ASTM D628-10. (2010). Standard test method for tensile properties of plastics. In
494 Annual book of ASTM standards. Philadelphia: American Society for Testing and
495 Materials.
496 Avérous, L., Fauconnier, N., Moro, L., and Fringant, C. (2000). Blends of thermoplastic
497 starch and polysteramide: processing and properties. *Journal of Applied Polymer*
498 *Science*, 1117-1128.
499 Azizi Samir. M.A.S., Alloin . F., and Dufresne, A. (2005) Review of recent research
500 into cellulosic whiskers, their properties and their application in nanobiocomposite
501 field. *Biomacromolecules*, 6(2), 612–626.
502 Bristol, J. H. (1986). Films, plastic. In M. Bakker (Ed.), *The Wiley encyclopedia of*
503 *packaging technology* (pp. 329–335). New York: 10, 1500–1507. Wiley
504 Cao, X., Chen, Y., Chang, P. R., Muir, A.D. and Falk, G. (2008). Starch-based
505 nanocomposites reinforced with flax cellulose nanocrystals. *Express Polymer Letters,* 2,
506 502-510.
507 Carmona, V.B., De Campos, A., Marconcini, J.M., Mattoso L.H.C. (2014). Kinetics of
508 thermal degradation applied to biocomposites with TPS, PCL and sisal fibers by non-
509 isothermal procedures. *Journal of Thermal Analysis and Calorimetry*, 115, 153–160
510 Dean, K.M., Do, M. D., Petinakis, E. and Yu, L. (2008): Key interactions in
511 biodegradable thermoplastic starch/poly(vinyl alcohol)/montmorillonite micro- and
512 nanocomposites. *Composite Science and Technology*, 68, 1453-1462.
513 Fabra, M.J., López-Rubio, A. and Lagaron, J.M. (2015a). Effect of the film-processing
514 conditions, relative humidity and aging on wheat gluten films coated with electrospun
515 polyhydryalkanoate. *Food Hydrocolloids*, 44, 292-299.

516 Fabra, M.J., López-Rubio, A. and Lagaron, J.M. (2015b). Three-Layer Films Based on
517 Wheat Gluten and Electrospun PHA. *Food and Bioprocess Technology,* 8(11), 2330-
518 2340.
519 Fabra, M.J., Pérez-Masiá, R., Talens, P., Chiralt, A. (2011). Influence of the
520 homogenization conditions and lipid self-association on properties of sodium caseinate
521 based films containing oleic and stearic acids. *Food Hydrocolloids*, 25, 1112-1121.
522 Fabra, M. J., Talens, P., and Chiralt, A. (2009). Microstructure and optical properties of
523 sodium caseinate films containing oleic acid-beeswax mixtures. *Food Hydrocolloids*,
524 23(3), 676-683.
525 Fortunati, E., Armentano, I., Iannoni, A., Kenny, J.M. (2010). Development and thermal
526 behaviour of ternary PLA matrix composites. *Polymer Degradation and Stability*, 95
527 (11), 2200-2206.
528 George, J., Ramana, K.V., Bawa, A.S., and Siddaramaiah, M.R. (2011) Bacterial
529 cellulose nanocrystals exhibiting high thermal stability and their polymer
530 nanobiocomposites. *International Journal of Biological Macromolecules*, 48(1), 50–57.
531 George, J., and Siddaramaiah, M. R. (2012). High performance edible nanocomposite
532 films containing bacterial cellulose nanocrystals. *Carbohydrate Polymers,* 87 (3), 2031-
533 2037.
534 Jiménez, A., Fabra, M. J., Talens, P., and Chiralt, A. (2012a). Effect of re-crystallization
535 on tensile, optical and water vapour barrier properties of corn starch films containing
536 fatty acids. *Food Hydrocolloids*, 26, 302-310.
537 Jiménez, A., Fabra, M. J., Talens, P., and Chiralt, A. (2012b). Edible and biodegradable
538 starch films: A review. *Food Bioprocess Technology*, 5, 2058–2076.
539 Kvien, I., Sugiyama, J., Votrubec, M., and Oksman, K. (2007). Characterization of
540 starch based nanocomposites. *Journal of Material Science,* 42, 8163-8171.

Lai, S. M., Huang, C. K., and Shen, H. F. (2005). Preparation and properties of biodegradable poly(butylene succinate)/starch blends. *Journal of Applied Polymer Science*, 257-264.

Liew, C.-W., and Ramesh, S. (2015). Electrical, structural, thermal and electrochemical properties of corn starch-based biopolymer electrolytes. *Carbohydrate Polymers,* 124, 9694, 222-228

Martínez-Sanz, M., Lopez-Rubio, A., and Lagaron, J.M. (2013). Nanobiocomposites of ethylene vinyl alcohol copolymer with thermally resistant cellulose nanowhiskers by melt compounding (II): water barrier and mechanical properties. *Journal of Applied Polymer Science*, 128(3), 2197–2207

Martínez-Sanz, M., López-Rubio, A., and Lagaron, J. M. (2014). Dispersing bacterial cellulose nanowhiskers in polylactides via electrohydrodynamic processing. *Journal of Polymers and the Environment*, 22, 27-40.

Martínez-Sanz, M., Olsson, R. T., López-Rubio, A., and Lagarón, J. M. (2011). Development of electrospun EVOH fibres reinforced with bacterial cellulose nanowhiskers. Part I: Characterization and method optimization. *Cellulose*, 18 (2), 335-347.

Mendes, J.F., Paschoalin, R.T., Carmona, V.B., Sena Neto, A.R., Marques, A.C.P., Marconcini, J.M., Mattoso, L.H.C., Medeiros, E.S., Oliveira, J.E. (2016). Biodegradable polymer blends based on corn starch and thermoplastic chitosan processed by extrusion. *Carbohydrate Polymers*, 137, 452-458.

Mohan, T.P., and Kanny, K. (2016). Thermoforming studies of corn starch-derived biopolymer film filled with nanoclays. *Journal of Plastic Film and Sheeting,* 32 (2), 163-188

565 Müller, C. M. O., Laurindo, J. B., and Yamashita, F. (2011). Effect of nanoclay
566 incorporation method on mechanical and water vapor barrier properties of starch-based
567 films. *Industrial Crops and Podructs*, 33, 605–610.
568 Park, H.M., Li, X., Jin, C.Z., Park, C. Y., Cho, W. J., and Ha, C. S. (2002). Preparation
569 and properties of biodegradable thermoplastic starch/clay hybrids. *Macromolecular*
570 *Materials and Engineering,* 287, 553-558.
571 Van Soest, J. J. G., Hulleman, S. H. D., de Wit, D., and Vliegenthart, J. F. G.
572 (1996).Crystallinity in starch bioplastics. *Industrial Crops and Products*, 5, 11–22.
573 Xie, F., Pollet, E., Halley, P.J., Avérous, L. (2013). Starch-based nano-biocomposites.
574 *Progress in Polymer Science,* 38, 1590-1628.
575 Xu, Y. X., Kimb, K. M., Hanna, M. A., and Nag, D. (2005). Chitosan starch composite
576 film: preparation and characterization. *Industrial Crops and Products*, 21(2), 185-192.
577 Zeppa, C., Gouanvé, F., and Espuche, E. (2009). Effect of a plasticizer on the structure
578 of biodegradable starch/clay nanocomposites: thermal, water-sorption, and oxygen-
579 barrier properties. *Journal of Applied Polymer Science,* 112, 2044-2056.
580
581
582
583
584
585
586
587
588
589

Table 1. Composition of the multilayer structures

Table 2. Tensile properties (E: Elastic Modulus, TS: Tensile Strength and EAB: Elongation at Break), water vapour permeability (measured at 0-100% RH) and oxygen permeability values (measured at 80% RH) of the TPCS based films and its nanobiocomposites containing 2, 5, 10, 15 or 20 wt% BCNW.

Table 3. Internal transmittance (Ti) values measured at 550 nm, tensile properties (E: Elastic Modulus, TS: Tensile Strength and EAB: Elongation at Break), water vapour permeability (measured at 0-100% RH), oxygen permeability (measured at 80% RH) and contact angle values of the multilayer structures.

615 **Figure Captions**

616 **Figure 1.** Contact transparency images of TPCS based films and its nanobiocomposites
617 containing 2, 5, 10, 15 or 20 wt% BCNW.

618

619 **Figure 2.** Spectral distribution of internal transmittance (Ti) of the TCPS based films
620 and its nanobiocomposites.

621

622 **Figure 3.** Cross-section micrographs of the TPCS based films and its
623 nanobiocomposites containing 2, 5, 15 or 20 wt% BCNW. (scale marker 100 μm)

624

625 **Figure 4.** Images obtained from optical microscopy with polarized light of the TPCS
626 based films and its nanobiocomposites containing 2, 10, 15 or 20 wt% BCNW. (scale
627 marker 20 μm)

628

629 **Figure 5.** Cross-section images of multilayer structure prepared with TPCS-15%BCNW
630 as inner layer and PHB-BCNW as outer layers.

631

632 **Figure 6.** Contact transparency images of multilayer structures.

633

634

635

636

637

638

639

640 **Table 1**

Sample	Multilayer films	
	Inner layer	Coating layers
A	TPCS	PHB
B		PHB-15% BCNW
C	TPCS-15%BCNW	PHB
D		PHB-15% BCNW

641

642

643 **Table 2.**

Nanobiocomposite Film	E (MPa)	TS (MPa)	EAB (%)	WVP·10^{13} (Kg·m·Pa^{-1}· s^{-1}·m^{-2})	OP·10^{18} (m^3·m·Pa^{-1}·s^{-1}·m^{-2})
TPCS	77 (11)^{a}	11.2 (0.8)^{a}	7.3 (1.9)^{a}	15.52 (0.09)^{a}	41.0 (2.3)^{a}
TPCS-2%BCNW	243 (13)^{b}	12.5 (3.4)^{a}	6.9 (0.9)^{a}	8.73 (0.72)^{b}	25.0 (1.5)^{b}
TPCS-5%BCNW	266 (6)^{b}	10.2 (3.3)^{a}	6.2 (0.7)^{a}	8.26 (0.57)^{b}	8.40 (0.20)^{c}
TPCS-10%BCNW	358 (57)^{c}	11.3 (2.0)^{a}	6.8 (1.6)^{a}	7.40 (0.31)^{bc}	4.16 (0.11)^{d}
TPCS-15%BCNW	831 (74)^{d}	18.9 (2.9)^{b}	3.3 (0.6)^{b}	6.42 (0.31)^{c}	2.03 (0.15)^{e}
TPCS-20%BCNW	808 (65)^{d}	20.0 (2.0)^{b}	3.6 (0.6)^{b}	7.48 (0.12)^{bc}	2.86 (0.17)^{e}

644 Different letters (a–e) within the same column indicate significant differences ($p<0.05$) between samples.
645

646

647 **Table 3.**

Multilayer films		$T_{i\ 550nm}$	E (MPa)	TS (MPa)	EAB (%)	WVP·10^{13} (Kg·m·Pa^{-1}· s^{-1}·m^{-2})	OP·10^{18} (m^3·m·Pa^{-1}·s^{-1}·m^{-2})	Contact angle θ (°)
Inner layer	Outer layers							
TPCS	PHB	83.8	538 (10)^{a}	6.9 (0.1)^{a}	5.80 (0.62)^{a}	2.63 (0.03)^{a}	76.3 (3.1)^{a}	10.5 (2.1)^{a}
	PHB-15% BCNW	79.6	670 (40)^{b}	6.7 (0.8)^{a}	4.57 (0.43)^{b}	0.71 (0.01)^{b}	79.4 (2.2)^{a}	7.7 (2.5)^{a}
TPCS-15%BCNW	PHB	76.5	779 (73)^{bc}	6.8 (2.0)^{a}	4.95 (0.45)^{ab}	0.74 (0.04)^{b}	74.6 (4.5)^{a}	9.8 (3.3)^{a}
	PHB-15% BCNW	74.6	868 (32)^{c}	6.4 (0.9)^{a}	3.45 (0.20)^{c}	0.66 (0.01)^{b}	78.2 (1.9)^{a}	7.3 (2.2)^{a}

648 Different letters (a–c) within the same column indicate significant differences ($p<0.05$) between samples.
649

650

651

652

653

Figure 1.

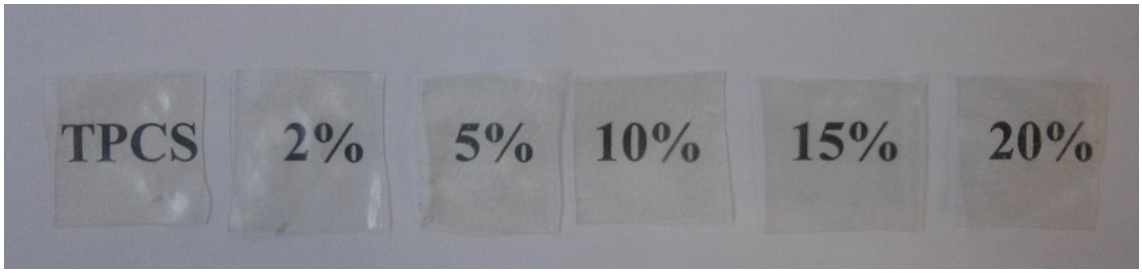

Figure 2.

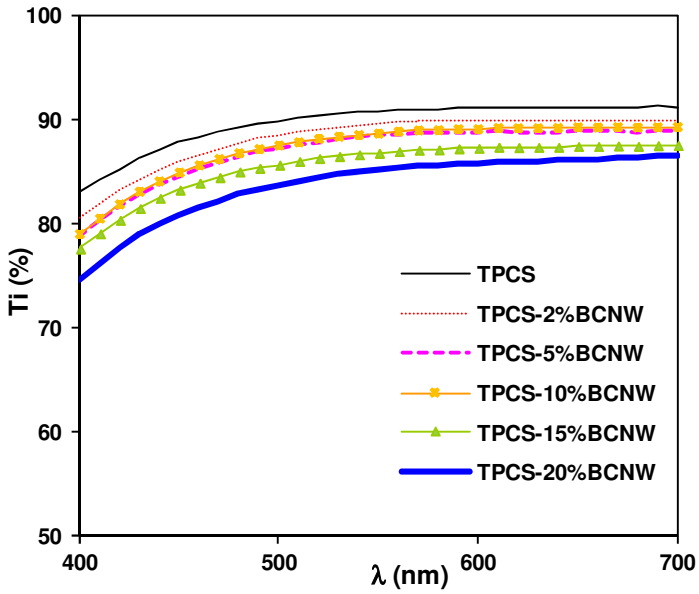
100
90
80
70
60
50
Ti (%)
400
500
600
700
λ (nm)
TPCS
TPCS-2%BCNW
TPCS-5%BCNW
TPCS-10%BCNW
TPCS-15%BCNW
TPCS-20%BCNW

Figure 3.

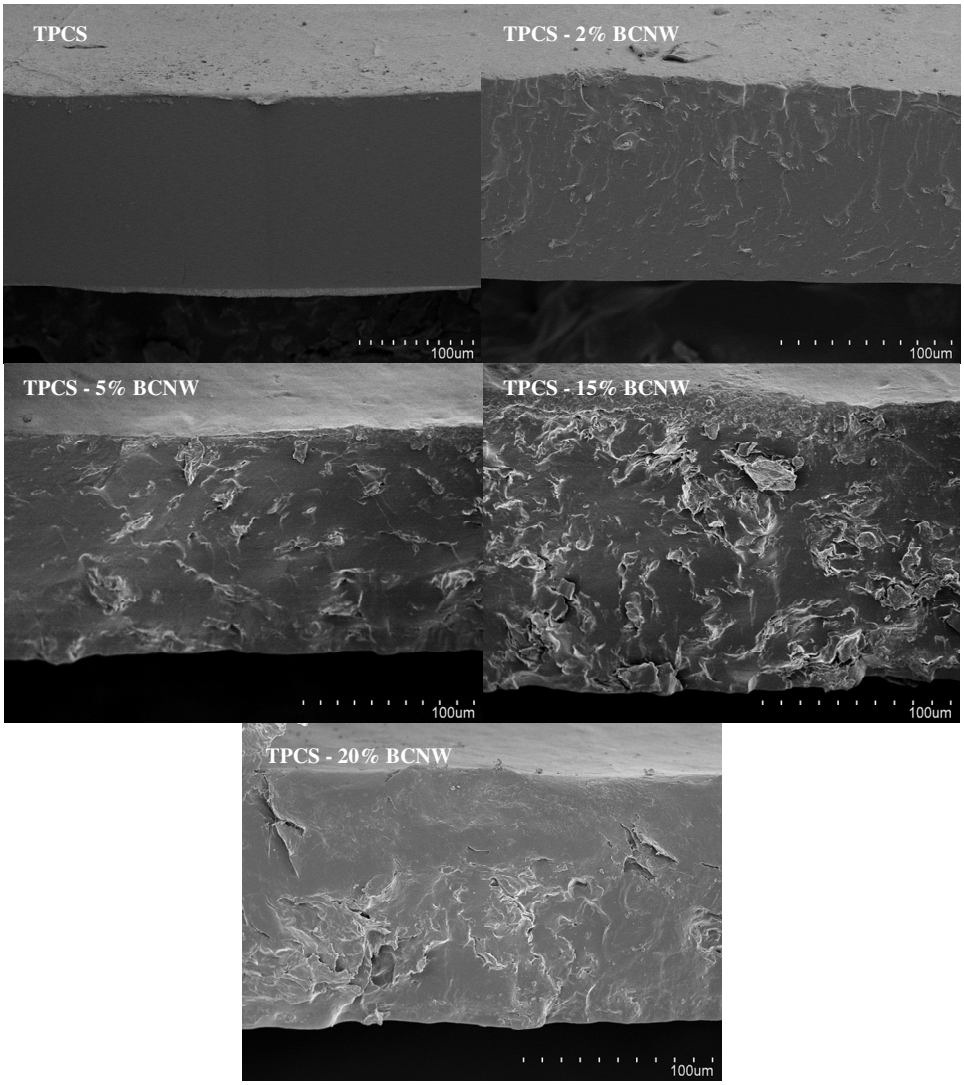
TPCS
100um
TPCS - 2% BCNW
100um
TPCS - 5% BCNW
100um
TPCS - 15% BCNW
100um
TPCS - 20% BCNW
100um

Figure 4.

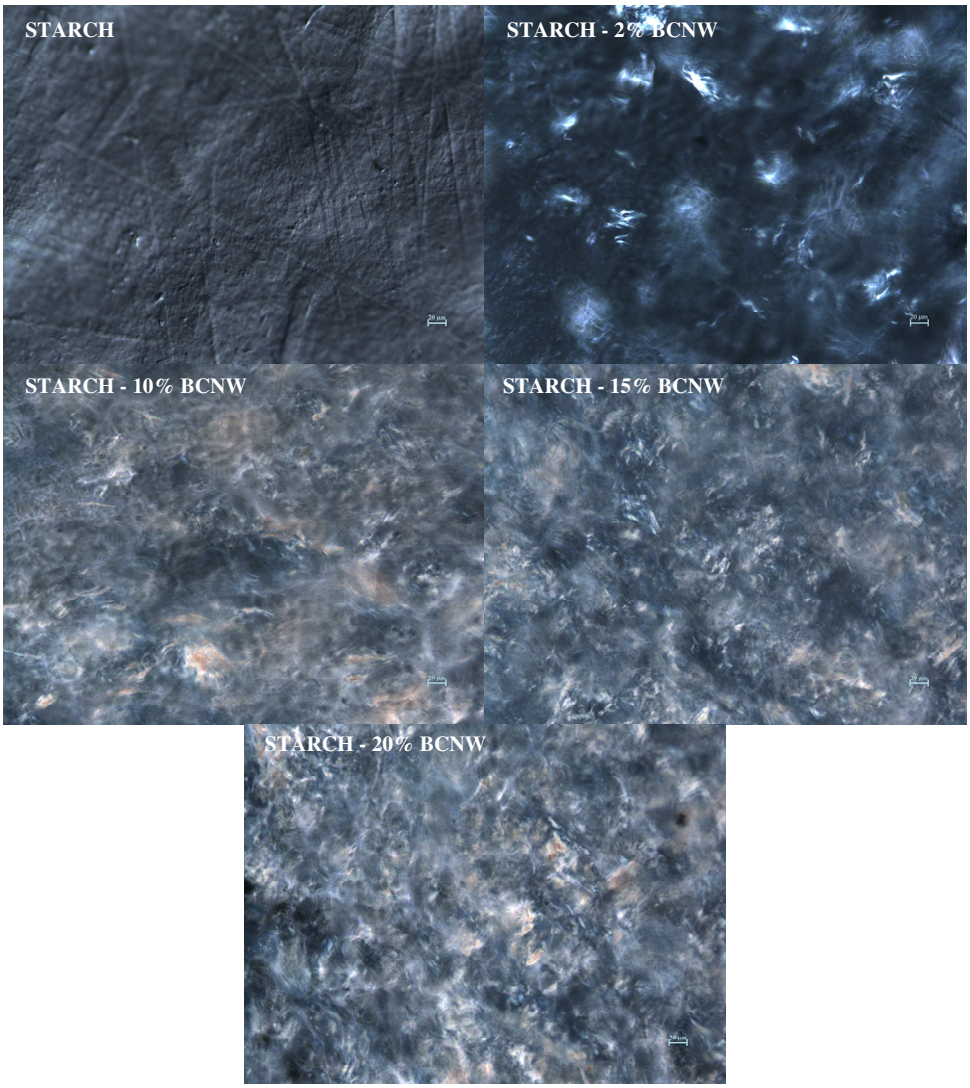
STARCH
STARCH - 2% BCNW
STARCH - 10% BCNW
STARCH - 15% BCNW
STARCH - 20% BCNW

Figure 5.

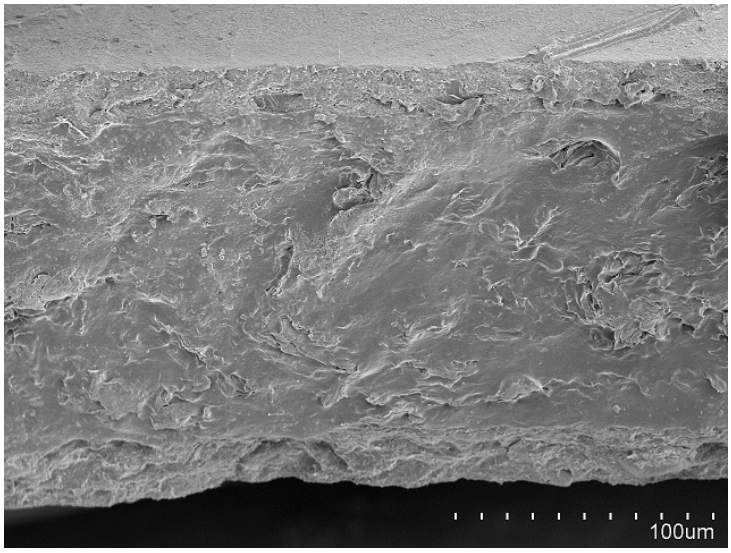

Figure 6.

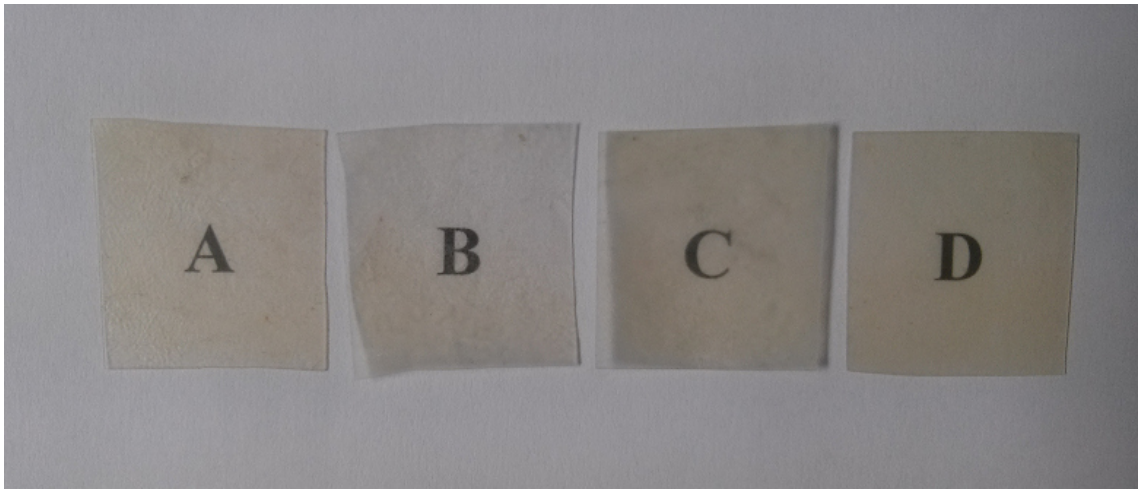

741
742 # Graphical Abstract

743 *María José Fabra*[*], *Amparo López-Rubio, Jesús, Ambrosio-Martín, Jose M. Lagaron*

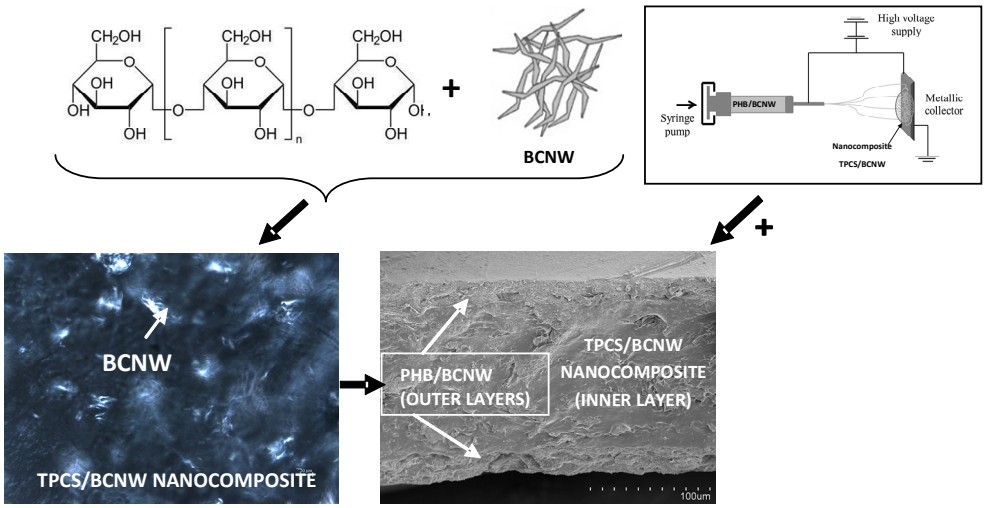

744
745